Multi-time-step Rolling Optimization Strategy for Post-disaster Emergency Recovery in Distribution System Based on Model Predictive Control

Haiyang Wan, *Student Member*, *IEEE*, Wenxia Liu, *Member*, *IEEE*, Qingxin Shi, *Member*, *IEEE*, Yiwei Zhang, Yuehan Wang, *Student Member*, *IEEE*, and Shuai Zhang

***Abstract*—Aimed at improving the resilience of distribution systems and analyzing the influence of uncertainties on the post-disaster emergency recovery process of a power-transportation system, this paper proposes a multi-time-step rolling optimization strategy based on model predictive control (MPC). First, the prediction models for three types of uncertainties: recovery time of faulty equipment, load demand and photovoltaic output are established. When it is assumed that traffic flow and density can meet a specific relationship, the cell transmission model (CTM) can be used to establish the transportation network. The evidence theory is used to model and analyze the two types of uncertain factors that constitute fault recovery time: travel time and repair time. Second, a mixed integer linear programming model of emergency recovery is established, in order to minimize load reduction and restoration resource scheduling cost. Decision variables include repair sequence of faulty equipment and the scheduling plan for restoration resources. Through the rolling optimization and feedback correction process, load demand can track the expected value and economic loss of power outages can be reduced as much as possible. Finally, a case study is used to verify the effectiveness of the method proposed in this paper and validate a multi-time-step rolling optimization strategy has the advantages of updating uncertain information multiple times, which can achieve the goal of planning a shorter path for the repair crew and shortening the total duration of fault recovery.**

***Index Terms*—Uncertainties, power-transportation system, model predictive control, resilience improvement, emergency recovery.**

NOMENCLATURE

A. Indices and Sets

$\Omega_{\mathrm{e}(i)}^{\mathrm{rep}(j)}$	Set of the predicted repair time of the faulty equipment $\mathrm{e}(i)$ by the No. j repair personnel.
Ω_{F}	Set of faulty equipment.
Ω_{TN}	Set of all cells in the transportation network.
t, Ω_{T1}	Index and set of time of the day.
$\Omega_{\mathrm{in}(i)/\mathrm{out}(i)}$	Set of the upstream and downstream cell of i.
$\Omega_{\mathrm{in}(j)/\mathrm{out}(j)}$	Set of the upstream and downstream node of j.
t, Ω_{T2}	Index and set of time of the entire emergency recovery period.
Ω_{CL}	Set of critical industrial load.
Ω_{NL}	Set of ordinary residential load.
Ω_{ES}	Set of energy storages.
Ω_{DG}	Set of distributed generators.
Ω_{L}	Set of loads.

B. Parameters

$F_i^{\max}$	Maximum flow into or out of cell i.
$\mu_i^{\max}$	Maximum flow that can be contained in cell i.
$o_i^{t_0}$	Flow in cell i at the initial time t_0.
$\zeta_{(i,j)}^{t_0}$	Flow from cell i to cell j at t_0.
l_i	Length of cell i.
v_i	Speed of repair crew freely passes through cell i.
c_{CL}	Unit reduction cost of critical industrial load.
c_{NL}	Unit reduction cost of ordinary residential load.
c_{ES}	Unit cost of charging of the energy storage.
$P_{\mathrm{L}}^{t,\mathrm{norm}}$	Normal active load demand of load L at t.
c_{DG}	Unit output cost of the distributed generator.
N_{crew}	Number of repair crews.
$P_{\mathrm{ES}(i)}^{\min\,/\,\max}$	Minimum and maximum power of the i-th energy storage can be absorbed or released in unit time.
$E_{\mathrm{ES}(i)}^{\max}$	Maximum capacity of the i-th energy storage.
$\mathrm{SOC}_{\mathrm{ES}(i)}^{\min\,/\,\max}$	Minimum and maximum state of charge of the i-th energy storage.
$P_{\mathrm{DG}(i)}^{\min\,/\,\max}$	Minimum and maximum power of the i-th distributed generator can supply.
$Rp_i^{\min\,/\,\max}$	Minimum and maximum value of the ramp rate of the i-th distributed generator.
$N_{(i,j)}^{\max}$	Maximum operations times of line (i,j).
$R_{(i,j)}/X_{(i,j)}$	Resistance and reactance of line (i,j).
$S_{(i,j)}$	Capacity of line (i,j).
$V_j^{\min\,/\,\max}$	Minimum and maximum voltage of node j.
N_{B}	Total number of passive nodes in the lossless virtual network.

Manuscript received October 31, 2021; revised January 10, 2022; accepted Apirl 11, 2022. Date of online publication August 18, 2022; date of current version October 24, 2022. This work was supported by the Fundamental Research Funds for the Central Universities (2021MS008).

H. Y. Wan, W. X. Liu, Q. X. Shi (corresponding author, emails: qshi@ncepu.edu.cn), Y. W. Zhang, Y. H. Wang and S. Zhang are with the College of Electrical and Electronics Engineering, North China Electric Power University. Beijing 102206, China.

DOI: 10.17775/CSEEJPES.2021.08050

C. Continuous Variables

$T^{\mathrm{rep}}_{\mathrm{e}(i)}$ Predicted repair time of the faulty equipment $\mathrm{e}(i)$.
$T^{t,\mathrm{tra}}_{(\mathrm{e}(i-1),\mathrm{e}(i))}$ Predicted travel time of the repair crew from the faulty equipment $\mathrm{e}(i-1)$ to $\mathrm{e}(i)$.
$T^{t}_{(\mathrm{e}(i-1),\mathrm{e}(i))}$ Predicted recovery time of the faulty equipment $\mathrm{e}(i)$.
$T^{t}_{(\mathrm{e}(i-1),\mathrm{e}(i))^{\alpha}}$ Actual recovery time of the faulty equipment $\mathrm{e}(i)$ under the confidential level α.
μ^t_i Predicted value of the traffic flow of cell i at t.
$f^t_{(k,i)}$ Predicted value of the flow from cell k to cell i at t.
s^t_i Actual traffic flow of cell i at t.
τ^t_i Actual travel time of the repair crew through cell i at t.
P^t_L Actual active load demand of load L at t.
$P^t_{\mathrm{ES}(i)}$ Power absorbed or released by the i-th energy storage at t, (positive value if is in the discharge state, 0 otherwise).
$P^t_{\mathrm{DG}(i)}$ Power generated by the i-th distributed generator at t.
$E^t_{\mathrm{ES}(i)}$ Capacity of the i-th energy storage at t.
$P^t_{(i,j)}$ Active power flow of the line (i,j) at t.
$P^t_{\mathrm{PV}(i)}$ Power generated by the i-th photovoltaic at t.
$Q^t_{(i,j)}$ Reactive power flow of the line (i,j) at t.
Q^t_L Reactive load demand of load L at t.
$F^t_{(i,j)}$ Virtual power flow of line (i,j) at t.

D. Binary Variables

$p^t_{\mathrm{e}(i)}$ Repair state variable of faulty equipment $\mathrm{e}(i)$ at time t (1 if being repaired by a crew, 0 otherwise).
$r^t_{\mathrm{e}(i)}$ Outage state variable of faulty equipment $\mathrm{e}(i)$ at time t (1 if having been repaired, 0 otherwise).
$q^t_{\mathrm{e}(i)}$ Outage state change variable of faulty equipment $\mathrm{e}(i)$ at t (1 if $r^{t-1}_{\mathrm{e}(i)}=0$, and $r^t_{\mathrm{e}(i)}=1$, 0 otherwise).
$w^t_{(i,j)}$ Switching state of the line (i,j) at time t (1 if is in the closed state, 0 otherwise).
$x^t_{(i,j)}$ Action state of the switch of the line (i,j) at time t (1 if $w^{t-1}_{(i,j)} \neq w^t_{(i,j)}$, 0 otherwise).

I. Introduction

In recent years, extreme weather events like ice disasters, typhoons, flood, etc., have occurred frequently, which has led to large-scale blackouts in the distribution system. For example, in February 2021, the extreme cold weather in Texas, USA caused the loss of more than 20,000 MW of load and affected a population of about 4 million [1]. Since the distribution system is coupled with other urban infrastructures, the loss of power supply has caused increasingly serious social unrest and economic losses [2].

In order to improve the defense and recovery capability of the distribution system against such low-probability-high-impact disasters, scholars have made great efforts on repair of faulty equipment and the restoration of critical load [3], [4]. In view of load restoration in the distribution system, numerous studies have been conducted in recent years. Emergency restoration resources have expanded from remote/manual switches [5]–[8], diesel generators [6], [7], [9] and batteries [10] to more flexible mobile emergency generators [11], [12], mobile energy storage [13]–[17] and micro energy grids [7], [10], etc. These restoration resources can form active islands and supply critical loads. Reference [17] proposes a pre-disaster allocation and post-disaster dispatch strategy of mobile energy storage for load restoration, which improves resilience of distribution system greatly. However, due to the temporal-coupling relationship between fault repair and load restoration [18], it is not enough to consider the process of load restoration alone. Also, the dynamic characteristics of emergency recovery will be affected by uncertainties such as power supply, load demand, and traffic flow. Therefore, current research focuses on 1) how to coordinate fault repair and load restoration, and 2) how to deal with uncertainties in emergency recovery.

Aimed at the first problem, existing research usually assumes that the repair time of faulty equipment is constant, and optimize the repair sequence and load restoration by using the following two methods: first is single-time-section optimization strategy (STSS), which means deciding the order of fault repair in a single time section based on prediction information of uncertainties after the disaster [9]. Once fault equipment is repaired, the operator conducts network reconfiguration and optimizes the recovery plan. However, when there are many faulty equipments affected by the disaster and the recovery duration is very long, ignoring the time variability of uncertainties will lead to the loss of the optimality of a recovery plan. Second is the multiple-time-section optimization strategy (MTSS), which means optimizing single faulty equipment that needs repair and the scheduling plan of restoration resources based on the ability of the repair crews and real-time updated system information [8]–[12]. Although MTSS makes better use of the latest information, it is partial optimization of each time section in theory and cannot achieve global optimal scheduling for equipment with temporal-coupling characteristics such as energy storage. In response to this problem, reference [19] adopts a model predictive control (MPC) algorithm. In each time section, the decision maker optimizes the load restoration plan in multiple time steps, but only executes the restoration plan of the first-time step; the process is repeated until the load is restored. It is concluded the load restoration process based on MPC can reduce more load shedding than STSS does. However, it fails to consider this process in conjunction with fault repairs.

In response to the second problem, the uncertainties considered in existing research mainly include travel time of repair crews [20], repair time of faulty equipment [21], [22] and load demand [21], [22]. Also, mathematical methods include robust optimization [20] and stochastic optimization [21]. Reference [20] establishes a two-stage robust optimization model. Under the worst conditions of the repair crews' travel time, it decides the repair sequence and scheduling plan of restoration resources in a single time section, which can minimize load shedding and total emergency recovery time. In [21], lognormal distribution and load prediction error are used to describe the probability distribution of repair time and

load demand, respectively. It uses Monte Carlo sampling to generate random scenarios and decides the repair plan under each scenario at a single step. There are two shortcomings in the above research: on one hand, it only fits uncertainties' probability model based on their historical data, and ignores uncertainties are changing over time during the actual disaster process. On the other hand, the modelling of recovery time is relatively rough, and it does not involve correlation analysis of travel time, travel path and traffic network congestion. When considering the variability of travel time, the predicted recovery time of each fault is changed since the starting position of repair crews and traffic flow are not fixed at different times. As a result, the remaining fault repair sequence and restoration resources scheduling plan should be modified.

To this end, this paper establishes prediction models that consider the uncertainties of the transportation system in post-disaster emergency recovery and proposes a new multi-time-step rolling optimization strategy based on MPC (MTSRS). Innovation points mainly include two aspects.

- First, by using the evidence theory and cell transmission model, prediction models for three uncertainties are established, including recovery time of faulty equipment, load demand and photovoltaic output.
- Second, a mixed integer linear programming model of emergency recovery is established based on the MPC, in order to minimize load reduction and restoration resource scheduling cost. The emergency recovery method is appliable to complex external environments and new restoration resources.

The remainder of this paper is organized as follows. Section II explains the research framework of emergency recovery based on MPC. In Section III, prediction models of uncertainties are established based on evidence theory. Section IV proposes MTSRS for fault repair and load restoration. The specific solution process is shown in Section V. Section VI provides the numerical analysis for illustrating the proposed method. Conclusions are given in Section VII.

II. Research Framework

A. Optimization Model Based on MPC

Model predictive control is also called rolling time domain control, and its basic model is shown in (1)–(2) [23]. The basic flowchart of MPC is shown in Fig. 1.

$$\boldsymbol{x}^{t+\Delta t} = \boldsymbol{A}\boldsymbol{x}^t + \boldsymbol{B}\boldsymbol{u}^t + \boldsymbol{C}\boldsymbol{d}^t \tag{1}$$

$$\boldsymbol{y}^t = \boldsymbol{D}\boldsymbol{x}^t \tag{2}$$

where $\boldsymbol{A}$, $\boldsymbol{B}$, $\boldsymbol{C}$, and $\boldsymbol{D}$ are the state space matrix, respectively; $\boldsymbol{r}^t$ is the expected output vector; $\boldsymbol{u}^t$ is the control input vector; $\boldsymbol{x}^t$ is the state vector; $\boldsymbol{d}^t$ is the disturbance input vector; $\boldsymbol{y}^t$ is the output vector; $\boldsymbol{x}^{t+\Delta t}$ is the state vector of the next time step.

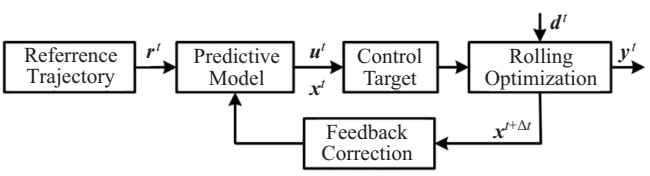

Fig. 1. Basic flowchart of MPC.

B. Rolling Optimization Model Based on MPC

Emergency recovery often takes hours or even days, during which period the traffic flow, load demand, photovoltaic output and topology of a distribution system will change over time. Timely use of updated information is a prerequisite to ensure accuracy of the recovery strategy. This paper proposes an improved MPC model suitable for prediction of uncertainties and post-disaster emergency recovery. The overall flowchart is shown in Fig. 2. According to the ultra-short-term forecast information of recovery time, load demand and photovoltaic output, the decision maker solves the restoration resource scheduling and fault repair sequence with the goal of minimizing operation costs. Meanwhile, only the first step of the scheduling plan is executed. Then, the above process repeats before the next time step. At the same time, a feedback correction process is conducted according to the latest information. Therefore, the load can track the expected value and load reduction is minimized.

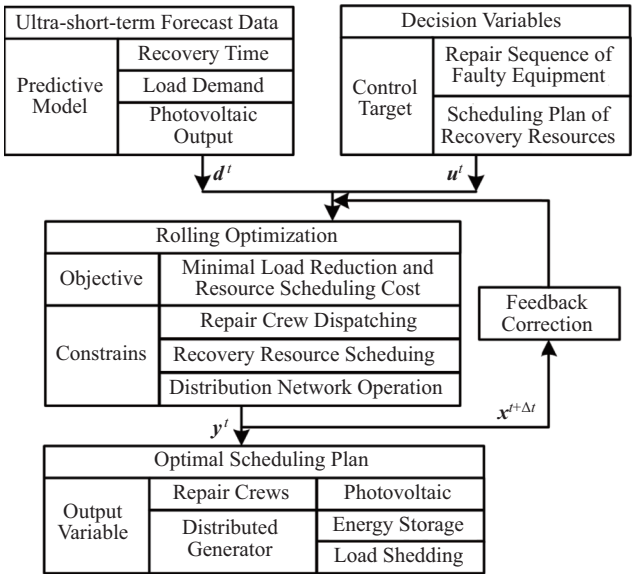

Fig. 2. Flowchart of emergency recovery based on MPC.

III. Stage I: Prediction Models of Uncertainties

The process of emergency recovery involves three uncertainties: recovery time of faulty equipment, load demand and photovoltaic output. Among them, forecast information of load and photovoltaic comes from the ultra-short-term forecast, and the forecast model is shown in (1) and (2). Prediction of faulty equipment recovery time consists of repair time and travel time. This article uses evidence theory to establish prediction models for these two types of uncertain factors [24].

A. Prediction Model of Repair Time

On one hand, repair time of faulty equipment is closely related to the experience of repair personnel. On the other hand, there are a large number of repair personnel that need

to be dispatched during the repair process and the working efficiency of different personnel vary. As a result, this subsection adopts evidence theory to construct and synthesize the predicted repair time structure of each repair personnel.

1) Evidence Structure of a Single Personnel

Let $\Omega_{\mathrm{e}(i)}^{\mathrm{rep}(1)}$ be the set of numerical distribution intervals of the predicted repair time $T_{\mathrm{e}(i)}^{\mathrm{rep}(1)}$, which can be expressed as $\Omega^{\mathrm{rep}(1)}\mathrm{e}(i) = \left\{\left[T_{\mathrm{e}(i),1,\min}^{\mathrm{rep}(1)}, T_{\mathrm{e}(i),1,\max}^{\mathrm{rep}(1)}\right], \left[T_{\mathrm{e}(i),2,\min}^{\mathrm{rep}(1)}, T_{\mathrm{e}(i),2,\max}^{\mathrm{rep}(1)}\right], \cdots, \left[T_{\mathrm{e}(i),f,\min}^{\mathrm{rep}(1)}, T_{\mathrm{e}(i),f,\max}^{\mathrm{rep}(1)}\right]\right\}$. Each interval in the set is called a focal element, and f is the number of focal elements. Each focal element has corresponding probability $p = \left[p_{\mathrm{e}(i),1}^{\mathrm{rep}(1)}, p_{\mathrm{e}(i),2}^{\mathrm{rep}(1)}, \cdots, p_{\mathrm{e}(i),f}^{\mathrm{rep}(1)}\right]$. When the focal element set and its corresponding probability are combined, evidence is formed. Taking the No. 1 personnel as an example, the evidence structure is shown in (3).

$$T_{\mathrm{e}(i)}^{\mathrm{rep}(1)} \in \begin{cases} \left[T_{\mathrm{e}(i),1,\min}^{\mathrm{rep}(1)}, T_{\mathrm{e}(i),1,\max}^{\mathrm{rep}(1)}\right] & p = p_{\mathrm{e}(i),1}^{\mathrm{rep}(1)} \\ \left[T_{\mathrm{e}(i),2,\min}^{\mathrm{rep}(1)}, T_{\mathrm{e}(i),2,\max}^{\mathrm{rep}(1)}\right] & p = p_{\mathrm{e}(i),2}^{\mathrm{rep}(1)} \\ \vdots & \\ \left[T_{\mathrm{e}(i),f,\min}^{\mathrm{rep}(1)}, T_{\mathrm{e}(i),f,\max}^{\mathrm{rep}(1)}\right] & p = p_{\mathrm{e}(i),f}^{\mathrm{rep}(1)} \end{cases}$$
$$\forall \mathrm{e}(i) \in \Omega_{\mathrm{F}} \tag{3}$$

Taking the first row of evidence as an example, this row represents the probability that predicted repair time of the faulty equipment $\mathrm{e}(i)$ by the No. 1 personnel is in the interval $\left[T_{\mathrm{e}(i),1,\min}^{\mathrm{rep}(1)}, T_{\mathrm{e}(i),1,\max}^{\mathrm{rep}(1)}\right]$ is $p_{\mathrm{e}(i)}^{\mathrm{rep}(1)}$.

2) Multiple Repair Personnel Evidence Synthesis

Evidence theory can be used to synthesize multiple sets of evidence. Taking the synthesis of two sets of evidence as an example, the rules are shown in (4) and (5).

$$p_{\mathrm{e}(i)}^{\mathrm{rep}}\left(T_{\mathrm{e}(i)}^{\mathrm{rep}}\right) = \frac{1}{K} \sum_{T_{\mathrm{e}(i)}^{\mathrm{rep}(1)} \cap T_{\mathrm{e}(i)}^{\mathrm{rep}(2)} = T_{\mathrm{e}(i)}^{\mathrm{rep}}} p_{\mathrm{e}(i)}^{\mathrm{rep}(1)}\left(T_{\mathrm{e}(i)}^{\mathrm{rep}(1)}\right) \times p_{\mathrm{e}(i)}^{\mathrm{rep}(2)}\left(T_{\mathrm{e}(i)}^{\mathrm{rep}(2)}\right) \tag{4}$$

$$K = \sum_{T_{\mathrm{e}(i)}^{\mathrm{rep}(1)} \cap T_{\mathrm{e}(i)}^{\mathrm{rep}(2)} \neq \varnothing} p_{\mathrm{e}(i)}^{\mathrm{rep}(1)}\left(T_{\mathrm{e}(i)}^{\mathrm{rep}(1)}\right) \times p_{\mathrm{e}(i)}^{\mathrm{rep}(2)}\left(T_{\mathrm{e}(i)}^{\mathrm{rep}(2)}\right) \tag{5}$$

where the faulty equipment satisfies $\mathrm{e}(i) \in \Omega_{\mathrm{F}}$; $p_{\mathrm{e}(i)}^{\mathrm{rep}}(T_{\mathrm{e}(i)}^{\mathrm{rep}})$ is the probability value corresponding to each focal element; K is the normalization factor. The larger the K, the smaller the conflict of each set of evidence.

B. Prediction Model of Travel Time

Due to the randomness of traffic flow of each road at different times, the time for vehicles to pass the same road in each time period is different. Based on this, this subsection predicts traffic flow first, and then constructs the travel time structure based on evidence theory.

1) Prediction Model of Traffic Flow

Using the cell transmission model to establish a transportation network model can solve the problem of uncertainty in traffic flow [25]. The theory proposes that when traffic network flow and density meet a certain relationship, time can be divided into multiple tiny intervals. At this time, the continuous transportation network can be divided into cells with length and direction. Length represents the distance the vehicle can travel freely in a unit time. Direction of the cell is the direction of the road. Based on this theory, the structure of a transportation network is equivalent to the cell structure, as shown in Fig. 3.

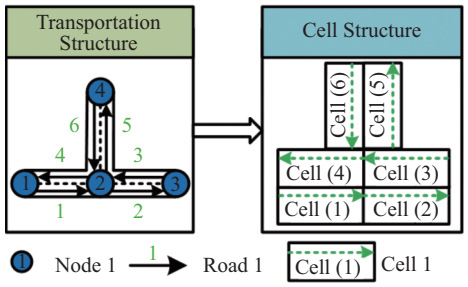

Fig. 3. The cell transmission model of the transportation network.

According to Wardrop's second balance principle (System Optimization): Based on the balance of the transportation network, traffic flow should be allocated according to the lowest total travel cost. Therefore, after converting the road structure of the traffic network into a cell structure, the objective function can be defined as minimizing the sum of traffic flows in all cells [26], as in (6).

$$\min \sum_{i \in \Omega_{\mathrm{TN}}} \sum_{t \in \Omega_{\mathrm{T1}}} \mu_i^t \tag{6}$$

Then, according to traffic flow at the current time, traffic flow in the next time window could be predicted under the constraints of (7)–(12).

$$\mu_i^{t+1} - \mu_i^t = \sum_{k \in \Omega_{\mathrm{in}(i)}} f_{(k,i)}^t - \sum_{j \in \Omega_{\mathrm{out}(i)}} f_{(i,j)}^t \tag{7}$$

$$\sum_{j \in \Omega_{\mathrm{out}(i)}} f_{(i,j)}^t \leq \mu_i^t \tag{8}$$

$$\sum_{k \in \Omega_{\mathrm{in}(i)}} f_{(i,j)}^t \leq F_i^{\max} \tag{9}$$

$$\sum_{j \in \Omega_{\mathrm{out}(i)}} f_{(i,j)}^t \leq F_i^{\max} \tag{10}$$

$$\sum_{k \in \Omega_{\mathrm{in}(i)}} f_{(i,j)}^t \leq \mu_i^{\max} - \mu_i^t \tag{11}$$

$$\mu_i^{t_0} = o_i^{t_0}, \ f_{(i,j)}^{t_0} = \zeta_{(i,j)}^{t_0} \tag{12}$$

where, the cells all satisfy $i \in \Omega_{\mathrm{TN}}$, and time variables all satisfy $t \in \Omega_{\mathrm{T1}}$.

When traffic flow μ_i^t of each cell is predicted according to (6)–(12), it is assumed the error between the predicted value and the actual value s_i^t obeys a normal distribution,

namely, $s_i^t \sim N(\mu_i^t, \sigma^2)$, where σ is the standard deviation. In order to construct the same structure as that of the predicted repair time, the probability density function of the actual value s_i^t is discretized. Let Ω_s be the set of numerical distribution intervals of s_i^t, which can be expressed as $\Omega_s = \{[s_{i,1,\min}^t, s_{i,1,\max}^t], \cdots, [s_{i,g,\min}^t, s_{i,g,\max}^t]\}$, where g is the number of focal elements. Taking the g-th focal element as an example, the probability of each focal element's value is shown in (13).

$$p_{s_{i,g}^t} = \int_{s_{i,g,\max}^t}^{s_{i,g,\min}^t} \frac{1}{\sqrt{2\pi}\sigma} \exp\left(-\frac{(s_i^t - \mu_i^t)^2}{2\sigma^2}\right) \mathrm{d}s_i^t \tag{13}$$

2) The Structure of Travel Time

According to the BPR road resistance function proposed by the Federal Highway Administration [27], traffic flow of various roads at each time can be converted into the actual travel time of vehicles on various roads, as shown in (14).

$$\tau_i^t = \frac{l_i}{v_i} \times \left(1 + \varepsilon \left(\frac{s_i^t}{\mu_i^{\max}}\right)^{\beta}\right) \tag{14}$$

where ε and β are the characteristic parameters of cell i, which are determined by the type of road corresponding to the cell.

Based on the actual travel time τ_i^t of the cell, the adjacency matrix A^t of the transportation network with time weight can be generated. When the starting position S^t and the ending position D^t of the repair crew at time t are known, the Dijkstra algorithm can be used to search for the shortest time $T_{(\mathrm{e}(i-1),\mathrm{e}(i))}^{t,\mathrm{tra}}$ of the repair crew from the faulty equipment $\mathrm{e}(i-1)$ to $\mathrm{e}(i)$, as shown in (15).

$$T_{(\mathrm{e}_{i-1},\mathrm{e}_i)}^{t,\mathrm{tra}} = \mathrm{Dijkstra}(A^t, S^t, D^t) \tag{15}$$

Let $\Omega_{(\mathrm{e}(i-1),\mathrm{e}(i))}^{t,\mathrm{tra}}$ be the set of numerical distribution intervals of the travel time $T_{(\mathrm{e}(i-1),\mathrm{e}(i))}^{t,\mathrm{tra}}$. Then

$$\begin{aligned}\Omega_{(\mathrm{e}(i-1),\mathrm{e}(i))}^{t,\mathrm{tra}} = \Big\{ &\left[T_{(\mathrm{e}(i-1),\mathrm{e}(i)),1,\min}^{t,\mathrm{tra}}, T_{(\mathrm{e}(i-1),\mathrm{e}(i)),1,\max}^{t,\mathrm{tra}}\right], \\ &\left[T_{(\mathrm{e}(i-1),\mathrm{e}(i)),2,\min}^{t,\mathrm{tra}}, T_{(\mathrm{e}(i-1),\mathrm{e}(i)),2,\max}^{t,\mathrm{tra}}\right], \cdots, \\ &\left[T_{(\mathrm{e}(i-1),\mathrm{e}(i)),g,\min}^{t,\mathrm{tra}}, T_{(\mathrm{e}(i-1),\mathrm{e}(i)),g,\max}^{t,\mathrm{tra}}\right]\Big\}\end{aligned}$$

where g is the number of focal elements. The probability calculation equation corresponding to each focal element is shown in (13), and the structure of $T_{(\mathrm{e}(i-1),\mathrm{e}(i))}^{t,\mathrm{tra}}$ is shown in (16).

$$T_{(\mathrm{e}(i-1),\mathrm{e}(i))}^{t,\mathrm{tra}} \in \begin{cases} \left[T_{(\mathrm{e}(i-1),\mathrm{e}(i)),1,\min}^{t,\mathrm{tra}}, T_{(\mathrm{e}(i-1),\mathrm{e}(i)),1,\max}^{t,\mathrm{tra}}\right] \\ \qquad\qquad p = p_{(\mathrm{e}(i-1),\mathrm{e}(i)),1}^{t,\mathrm{tra}} \\ \left[T_{(\mathrm{e}(i-1),\mathrm{e}(i)),2,\min}^{t,\mathrm{tra}}, T_{(\mathrm{e}(i-1),\mathrm{e}(i)),2,\max}^{t,\mathrm{tra}}\right] \\ \qquad\qquad p = p_{(\mathrm{e}(i-1),\mathrm{e}(i)),2}^{t,\mathrm{tra}} \\ \qquad\qquad \vdots \\ \left[T_{(\mathrm{e}(i-1),\mathrm{e}(i)),g,\min}^{t,\mathrm{tra}}, T_{(\mathrm{e}(i-1),\mathrm{e}(i)),g,\max}^{t,\mathrm{tra}}\right] \\ \qquad\qquad p = p_{(\mathrm{e}(i-1),\mathrm{e}(i)),g}^{t,\mathrm{tra}} \end{cases} \tag{16}$$

C. Prediction Model of Recovery Time

1) The Structure of Recovery Time

The set of joint probability density interval $\Omega_{(\mathrm{e}(i-1),\mathrm{e}(i))}^t$ is constructed by the Cartesian product operation, which is performed on the numerical probability distribution intervals of the two types of independent variables $T_{(\mathrm{e}(i-1),\mathrm{e}(i))}^{t,\mathrm{tra}}$ and T rep $\mathrm{e}(i)$, given by (17). The response boundary of each focal element and the corresponding probability are given by (18) and (19).

$$\begin{aligned}\Omega_{(\mathrm{e}(i-1),\mathrm{e}(i))}^t &= \Omega_{(\mathrm{e}(i-1),\mathrm{e}(i))}^{t,\mathrm{tra}} \times \Omega_{\mathrm{e}(i)}^{\mathrm{rep}} \\ &= \sum_{\forall f} \sum_{\forall g} T_{\mathrm{e}(i),f}^{\mathrm{rep}} \times T_{(\mathrm{e}(i-1),\mathrm{e}(i)),g}^{t,\mathrm{tra}}\end{aligned} \tag{17}$$

$$T_{(\mathrm{e}_{i-1},\mathrm{e}_i)}^t \in \begin{cases} \left[T_{(\mathrm{e}(i-1),\mathrm{e}(i)),1,\min}^t, T_{(\mathrm{e}(i-1),\mathrm{e}(i)),1,\max}^t\right] \\ \qquad\qquad p = p_{(\mathrm{e}(i-1),\mathrm{e}(i)),1}^t \\ \left[T_{(\mathrm{e}(i-1),\mathrm{e}(i)),2,\min}^t, T_{(\mathrm{e}(i-1),\mathrm{e}(i)),2,\max}^t\right] \\ \qquad\qquad p = p_{(\mathrm{e}(i-1),\mathrm{e}(i)),2}^t \\ \qquad\qquad \vdots \\ \left[T_{(\mathrm{e}(i-1),\mathrm{e}(i)),h,\min}^t, T_{(\mathrm{e}(i-1),\mathrm{e}(i)),h,\max}^t\right] \\ \qquad\qquad p = p_{(\mathrm{e}(i-1),\mathrm{e}(i)),h}^t \end{cases} \tag{18}$$

$$\begin{aligned}p_{(\mathrm{e}(i-1),\mathrm{e}(i))}^t = &\sum_{\forall f} \sum_{\forall g} p_{\mathrm{e}(i),f}^{\mathrm{rep}} \left(T_{\mathrm{e}(i),f}^{\mathrm{rep}}\right) \\ &\times p_{(\mathrm{e}(i-1),\mathrm{e}(i)),g}^{t,\mathrm{tra}} \left(T_{(\mathrm{e}(i-1),\mathrm{e}(i)),g}^{t,\mathrm{tra}}\right)\end{aligned} \tag{19}$$

where h is the number of focal elements and $h = g \times h$.

2) The Matrix of Recovery Time

Assume event γ is the predicted recovery time $T_{(\mathrm{e}(i-1),\mathrm{e}(i))}^t$ is not larger than the actual recovery time $T_{(\mathrm{e}(i-1),\mathrm{e}(i))^*}^t$, namely, $T_{(\mathrm{e}(i-1),\mathrm{e}(i))}^t \le T_{(\mathrm{e}(i-1),\mathrm{e}(i))^*}^t$. Define the credibility function of event γ as $\mathrm{Bel}(\gamma)$, which represents the degree of trust that event γ is established, and its value is shown in (20).

$$\mathrm{Bel}(\gamma) = \sum_{\forall h} p\left(T_{(\mathrm{e}(i-1),\mathrm{e}(i)),h,\max}^t \le T_{(\mathrm{e}(i-1),\mathrm{e}(i))^*}^t\right) \tag{20}$$

When the trust degree of the required event γ is not lower than the confidential level α, then (21) is established. Under this condition, recovery time, travel time and repair time are $T_{(\mathrm{e}(i-1),\mathrm{e}(i))^\alpha}^t$, $T_{(\mathrm{e}(i-1),\mathrm{e}(i))^\alpha}^{t,\mathrm{tra}}$ and $T_{\mathrm{e}(i)^\alpha}^{\mathrm{rep}}$ respectively.

$$\mathrm{Bel}(\gamma) \ge \alpha \tag{21}$$

Let Ω_{cell} be the set of the initial locations P_0 of the repair crews and the cells where each faulty equipment $\mathrm{e}(i)$ is located. Then, $\Omega_{\mathrm{cell}} = [\mathrm{cell}(P_0), \mathrm{cell}(\mathrm{e}(1)), \cdots, \mathrm{cell}(\mathrm{e}(i))]$. By repeatedly replacing the start and end positions in (15) with the elements in set Ω_{cell}, the recovery time matrix $[T_{(\mathrm{e}(i-1),\mathrm{e}(i))^\alpha}^t]$ under the confidential level α can be obtained, as shown in (22).

$$\left[T^t_{(\mathrm{e}(i-1),\mathrm{e}(i))^\alpha}\right] = \begin{array}{c} \\ P_0 \\ e(1) \\ \vdots \\ \mathrm{e}(i-1) \\ \mathrm{e}(i) \end{array} \begin{array}{c} \begin{array}{cccccc} P_0 & \mathrm{e}(1) & \cdots & \mathrm{e}(i-1) & \mathrm{e}(i) \end{array} \\ \begin{bmatrix} 0 & 12 & \cdots & 13 & 10 \\ 10 & 0 & \cdots & 13 & 10 \\ \vdots & \vdots & \ddots & \vdots & \vdots \\ 11 & 12 & \cdots & 0 & 10 \\ 10 & 11 & \cdots & 13 & 0 \end{bmatrix} \end{array} \tag{22}$$

IV. Stage II: Multi-time-step Rolling Optimization Strategy

In stage II, a mixed integer linear programming model is established to minimize load reduction and restoration resource scheduling cost. Constraints include repair crew dispatching, restoration resource scheduling and distribution network operation, The solution is obtained based on the rolling optimization and feedback correction in the MPC.

A. Objective Function

$$\begin{aligned} \min \quad & \sum_{t\in\Omega_{\mathrm{T2}}}\left(\sum_{L\in\Omega_{\mathrm{CL}}} c_{\mathrm{CL}}(P_{\mathrm{L}}^{t,\mathrm{norm}}-P_{\mathrm{L}}^{t})\right. \\ & +\sum_{L\in\Omega_{\mathrm{NL}}} c_{\mathrm{NL}}(P_{\mathrm{L}}^{t,\mathrm{norm}}-P_{\mathrm{L}}^{t}) \\ & \left.+\sum_{i\in\Omega_{\mathrm{ES}}} c_{\mathrm{ES}}P^t_{\mathrm{ES}(i)}+\sum_{L\in\Omega_{\mathrm{DG}}} c_{\mathrm{DG}}P^t_{\mathrm{DG}(i)}\right) \end{aligned} \tag{23}$$

The objective function (23) is mainly composed of four parts. The first two represent reduction of the two types of loads. The reason for accounting the third and fourth items is to avoid unnecessary work process of distributed generators and energy storages when the load is restored [17]. Since the values of the latter two are generally smaller than the first two, the main target of (23) is still seeking to minimize load reduction.

B. Repair Crew Dispatching Constraints

$$p^t_{\mathrm{e}(i)}=\begin{cases} 1 & t\in\left[t_{\mathrm{e}(i-1)}+T^{t,\mathrm{tra}}_{(\mathrm{e}(i-1),\mathrm{e}(i))^\alpha},t_{\mathrm{e}(i)}\right] \\ 0 & t\notin\left[t_{\mathrm{e}(i-1)}+T^{t,\mathrm{tra}}_{(\mathrm{e}(i-1),\mathrm{e}(i))^\alpha},t_{\mathrm{e}(i)}\right] \end{cases} \tag{24}$$

$$q^t_{\mathrm{e}(i)}=\begin{cases} 1 & t=t_{\mathrm{e}(i)} \\ 0 & t\neq t_{\mathrm{e}(i)} \end{cases} \tag{25}$$

$$r^t_{\mathrm{e}(i)}=\sum_t q^t_{\mathrm{e}(i)} \tag{26}$$

$$\sum_{\mathrm{e}(i)} p^t_{\mathrm{e}(i)}\le N_{\mathrm{crew}} \tag{27}$$

where all faulty equipment satisfies $\mathrm{e}(i)\in\Omega_{\mathrm{F}}$, and all time variables satisfy $t\in\Omega_{\mathrm{T2}}$. $t_{\mathrm{e}(i)}$ is the recovery time of faulty equipment $\mathrm{e}(i)$. $t_{\mathrm{e}(i)}$ is composed of the recovery time of the faulty equipment $\mathrm{e}(i-1)$ and the repair time of the faulty equipment $\mathrm{e}(i)$, namely $t_{\mathrm{e}(i)}=t_{\mathrm{e}(i-1)}+T^t_{(\mathrm{e}(i-1),\mathrm{e}(i))^\alpha}$.

In order to explain the dispatching constraints of the repair crews and application of MPC in the emergency repair process clearly, the decision-making and scheduling process at two layers of time and space is constructed as shown in Fig. 4.

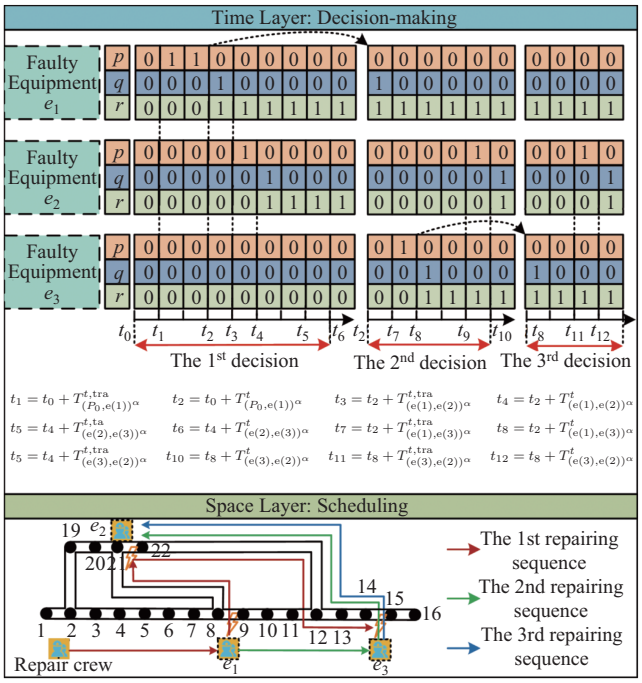

Fig. 4. MPC-based emergency repair crew scheduling illustration diagram.

Assuming there are three faulty equipment in the system at time t_0, the values of the state variables: $p^t_{\mathrm{e}(i)}$, $q^t_{\mathrm{e}(i)}$ and $r^t_{\mathrm{e}(i)}$, of each faulty equipment is displayed in the time layer, and the optimal repair sequence results of each faulty equipment is correspondingly displayed in the space layer.

In the first optimization decision at t_0, the crew will repair the faulty equipment in the order of $\mathrm{e}(1)\rightarrow\mathrm{e}(2)\rightarrow\mathrm{e}(3)$. The traffic path is shown by the red arrow in Fig. 4. The description of the emergency repair plan is as follows. To begin with, the crew travels from the initial location P_0 to the faulty equipment $\mathrm{e}(1)$ during the period $[t_0,t_1]$, and the repair process is completed at t_2. After that, the crew travels from the faulty equipment $\mathrm{e}(1)$ to $\mathrm{e}(2)$ in the period $[t_2,t_3]$, and repairs $\mathrm{e}(2)$ at time t_4. Finally, the crew repairs $\mathrm{e}(3)$ at t_6. However, travel time from $\mathrm{e}(1)$ to $\mathrm{e}(3)$ at time t_2 is predicted to decrease based on updated traffic flow information. After the second optimization decision, the crew will repair the remaining faulty equipment in the order of $\mathrm{e}(3)\rightarrow\mathrm{e}(2)$. The traffic path is shown by the green arrow in Fig. 4. The emergency repair plan is similar to the above description. Finally, after the third optimization decision, the crew completed all repair tasks at time t_{12}.

C. Restoration Resources Scheduling Constraints

In (28) to (48), the time variables all satisfy $t\in\Omega_{\mathrm{T2}}$, the lines of distribution network all satisfy $(i,j)\in\Omega_{\mathrm{L}}$, and the nodes of distribution network all satisfy $j\in\Omega_{\mathrm{DN}}$.

1) Energy Storage

$$P^{\min}_{\mathrm{ES}(i)}\le P^t_{\mathrm{ES}(i)}\le P^{\max}_{\mathrm{ES}(i)}\quad\forall i\in\Omega_{\mathrm{ES}} \tag{28}$$

$$E^{t+1}_{\mathrm{ES}(i)}=E^t_{\mathrm{ES}(i)}-P^t_{\mathrm{ES}(i)}\Delta t\quad\forall i\in\Omega_{\mathrm{ES}} \tag{29}$$

$$E^{\max}_{\mathrm{ES}(i)}\times\mathrm{SOC}^{\min}_{\mathrm{ES}(i)}\le E^t_{\mathrm{ES}(i)}\le E^{\max}_{\mathrm{ES}(i)}\times\mathrm{SOC}^{\max}_{\mathrm{ES}(i)}\quad\forall i\in\Omega_{\mathrm{ES}} \tag{30}$$

2) Distributed Generator

$$P^{\min}_{\mathrm{DG}(i)} \le P^{t}_{\mathrm{DG}(i)} \le P^{\max}_{\mathrm{DG}(i)} \quad \forall i \in \Omega_{\mathrm{DG}} \tag{31}$$

$$Rp^{\min}_{i} \le |P^{t+1}_{\mathrm{DG}(i)} - P^{t}_{\mathrm{DG}(i)}| \le Rp^{\max}_{i} \quad \forall i \in \Omega_{\mathrm{DG}} \tag{32}$$

3) Shedding Load

$$0 \le P^{t}_{\mathrm{L}} \le P^{t,\mathrm{norm}}_{\mathrm{L}} \ \forall L \in \Omega_{\mathrm{L}} \tag{33}$$

D. Distribution Network Operation Constraints

1) Active and Reactive Power Balance Constraints

$$\sum_{k\in\Omega_{\mathrm{out}(j)}} P^{t}_{(j,k)} - \sum_{i\in\Omega_{\mathrm{in}(j)}} P^{t}_{(i,j)} = \sum_{i\in\Omega_{\mathrm{ES}}} P^{t}_{\mathrm{ES}(i)} + \sum_{i\in\Omega_{\mathrm{PV}}} P^{t}_{PV(i)} + \sum_{i\in\Omega_{\mathrm{DG}}} P^{t}_{\mathrm{DG}(i)} - \sum_{L\in\Omega_{\mathrm{L}}} P^{t}_{\mathrm{L}} \tag{34}$$

$$\sum_{k\in\Omega_{\mathrm{out}(j)}} Q^{t}_{(j,k)} - \sum_{i\in\Omega_{\mathrm{in}(j)}} Q^{t}_{(i,j)} = \sum_{L\in\Omega_{\mathrm{L}}} Q^{t}_{\mathrm{L}} \tag{35}$$

2) Line Switch State Constraints

$$w^{t}_{(i,j)} \le r^{t}_{(i,j)} \tag{36}$$

$$w^{t}_{(i,j)} \ge x^{t+1}_{(i,j)} - x^{t}_{(i,j)} \tag{37}$$

$$w^{t}_{(i,j)} \ge x^{t}_{(i,j)} - x^{t+1}_{(i,j)} \tag{38}$$

$$\sum_{t\in\Omega_{\mathrm{T2}}} x^{t}_{(i,j)} \le N^{\max}_{(i,j)} \tag{39}$$

Constraint (36) represents when the line (i, j) is in a faulty state, the corresponding switch must be opened. When it is in the normal state, the switch can be closed or opened.

3) Linear DistFlow Constraint

This article uses the Linear DistFlow proposed in literature [28]–[31] and sets the system standard voltage $V_0 = 1$.

$$-M_1(1 - w^{t}_{(i,j)}) \le V^{t}_{i} - V^{t}_{j} - \left(\frac{R_{(i,j)}P^{t}_{(i,j)} + X_{(i,j)}Q^{t}_{(i,j)}}{V_0}\right) \le M_1(1 - w^{t}_{(i,j)}) \tag{40}$$

where M_1 is a very large positive number. When $w^{t}_{(i,j)} = 0$, namely, the switch of line (i, j) is opening, this constraint will no longer limit the relationship between node voltage and line power flow.

4) Line Capacity Constraints

$$\left(P^{t}_{(i,j)}\right)^2 + \left(Q^{t}_{(i,j)}\right)^2 \le \left(S_{(i,j)}\right)^2 \tag{41}$$

$$-w^{t}_{(i,j)}S_{(i,j)} \le P^{t}_{(i,j)} \le w^{t}_{(i,j)}S_{(i,j)} \tag{42}$$

$$-0.5w^{t}_{(i,j)}S_{(i,j)} \le Q^{t}_{(i,j)} \le 0.5w^{t}_{(i,j)}S_{(i,j)} \tag{43}$$

Considering that $P^{t}_{(i,j)} > Q^{t}_{(i,j)}$ generally exists in the distribution network, then the rectangular area represented by (42) and (43) can be used to replace the circular area in (43) [32].

5) Node Voltage Constraint

$$V^{\min}_{j} \le V^{t}_{j} \le V^{\max}_{j} \tag{44}$$

6) Radial Constraints

In the process of fault repair and load restoration, the topology of the distribution network needs to always maintain a radial topology. The single commodity flow (SCF) proposed in [33] can model radial topological condition as a set of linear constraints. A lossless virtual network with the same structure is constructed with the same line switch state as the original distribution network, as shown in Fig. A1. Under this condition, the radial constraint can be described by (45)–(48).

$$\sum_{(i,j)\in\Omega_{\mathrm{L}}} w^{t}_{(i,j)} \le N_{\mathrm{B}} \tag{45}$$

$$\sum_{k\in\Omega_{\mathrm{out}}(j)} F^{t}_{(j,k)} - \sum_{i\in\Omega_{\mathrm{in}}(j)} F^{t}_{(i,j)} = -1 \quad j \ne 1 \tag{46}$$

$$\sum_{k\in\Omega_{\mathrm{out}}(j)} F^{t}_{(j,k)} \le N_{\mathrm{B}} \quad j = 1 \tag{47}$$

$$-M_2 w^{t}_{(i,j)} \le F^{t}_{(i,j)} \le M_2 w^{t}_{(i,j)} \tag{48}$$

where, M_2 is a large positive number.

V. Solution Process

The specific solution process in this paper is shown in Fig. 5.

Stage I establishes prediction models of uncertainties. First, the load and photovoltaic output are obtained through intraday ultra-short-term forecasting. Second, the repair time of faulty equipment is synthesized through evidence theory. Third, by using the cell transmission model to construct the transportation network, traffic flow can be predicted. Then, search for the shortest path and travel time by using BPR model and Dijkstra algorithm. Finally generate recovery time.

Stage II develops a multi-time-step rolling optimization strategy for fault repair and load restoration. According to the forecast information of the uncertainties, the model predictive control is adopted to optimize the decision-making of the repair sequence and scheduling plan within this time window, but only the first step of the scheduling plan is executed. After that, judging whether the number of faulty equipment has decreased. If so, update the set of faults. If there is still faulty equipment, repeat the above process until all faults are repaired.

VI. Case Study

The computational tasks are performed on a personal laptop computer with an Intel Core i7 Processor (2.20 GHz) and 16-GB RAM, and the code is implemented via the Matlab-based YALMIP-CPLEX Optimization Studio V12.8.0. Set the time step as $\Delta t = 15$ min.

A. Test System

The distribution system adopts the modified IEEE 33-bus system, as shown in Fig. 6. There are three energy storages, four photovoltaic and two distributed generators connected. The remaining parameters of each unit are shown in Tables A1–A2. Assuming the distribution system is affected by extreme disaster at $t_0 = 44$, and there are four faulty equipment $\{\mathrm{e}(i)|(3,4),(7,8),(10,11),(22,23)\}$. The ultra-short-term forecast curves of loads demand and photovoltaic

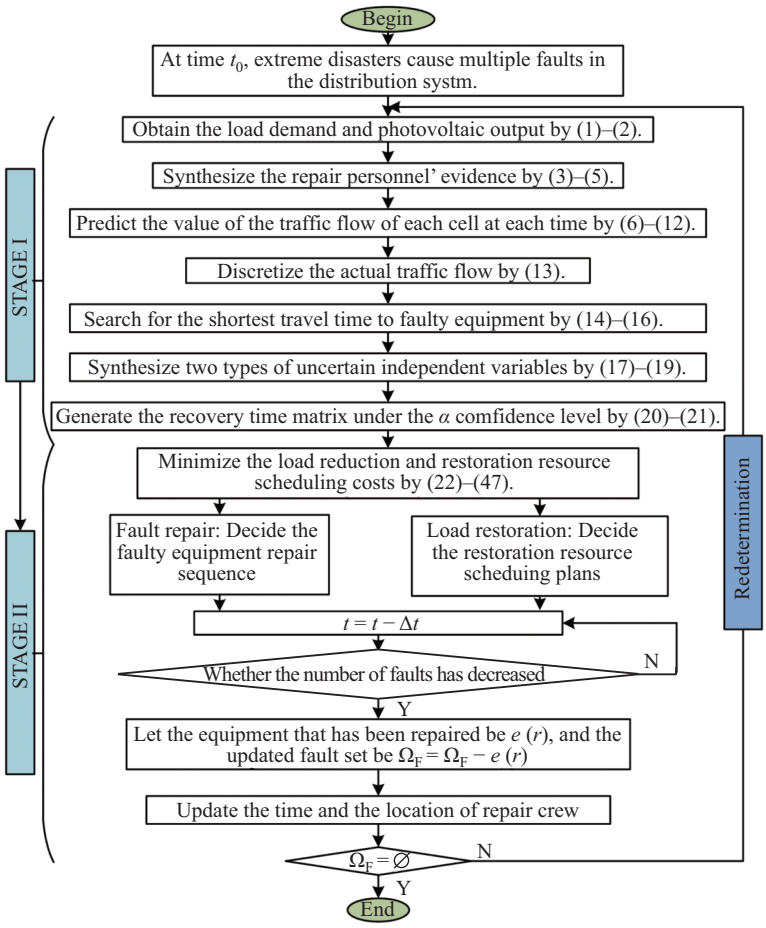

Fig. 5. Multi-time-step rolling optimization strategy process.

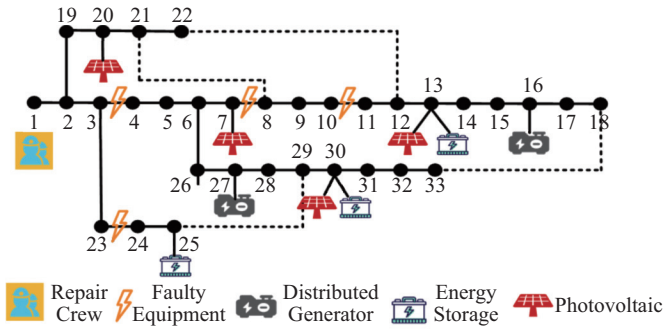

Fig. 6. The modified IEEE 33-bus system.

output are shown in Fig. A2, and cost reduction of the two types of loads are 1.5 and 0.5, respectively. The initial location of the repair crew is cell 1. The maximum number of switching operations is 3.

As shown in Fig. 7, the transportation system consists of 33 nodes and 72 roads. The roads are divided into express roads, main roads, sub-main roads and branch roads. The parameters of each road and its corresponding cell are shown in Table A3.

In addition, it is assumed that each faulty equipment is repaired by two personnel, the prediction process of repair time is shown in Table A4. The actual value of traffic flow with the predicted value is set to obey normal distribution and variance is 10%. Taking cell 1 as an example, the sub-intervals and probability values of the predicted traffic flow value at t_0 are shown in Table A5. The confidential level of the recovery time of the faulty equipment is $\alpha = 0.8$.

B. Results and Comparative Analysis of Different Strategies

1) Three Strategy Optimization Results

When MTSRS is adopted, through stage I, the predicted recovery time matrix at time $t_0 = 44$, $t = 53$, $t = 63$ and $t = 73$ is shown in Fig. B1, B2, B3 and B4, respectively. After multiple rolling decisions through stage II, the optimal repair sequence for the faulty equipment is $\mathrm{e}(1) \rightarrow \mathrm{e}(2) \rightarrow \mathrm{e}(3) \rightarrow \mathrm{e}(4)$, and it is estimated the repair will be completed, respectively, at time $t = 53$, $t = 63$, $t = 73$ and $t = 86$. The repair route, load reduction and number of faulty lines, output of distributed generators and charging/discharging of energy storages are shown in Figs. 8, 9 and 10, respectively. The predicted target value is \$17569.1, and the calculation time is 746.40 s.

When STSS is adopted, the recovery time matrix predicted at time $t_0 = 44$ is shown in Fig. B1. After a single decision through stage II, the optimal repair sequence is $\mathrm{e}(1) \rightarrow \mathrm{e}(4) \rightarrow \mathrm{e}(2) \rightarrow \mathrm{e}(3)$, and it is estimated the repair will be completed respectively at time $t = 53$, $t = 65$, $t = 77$ and $t = 87$. The repair route is shown in Fig. 8(a). Load reduction and

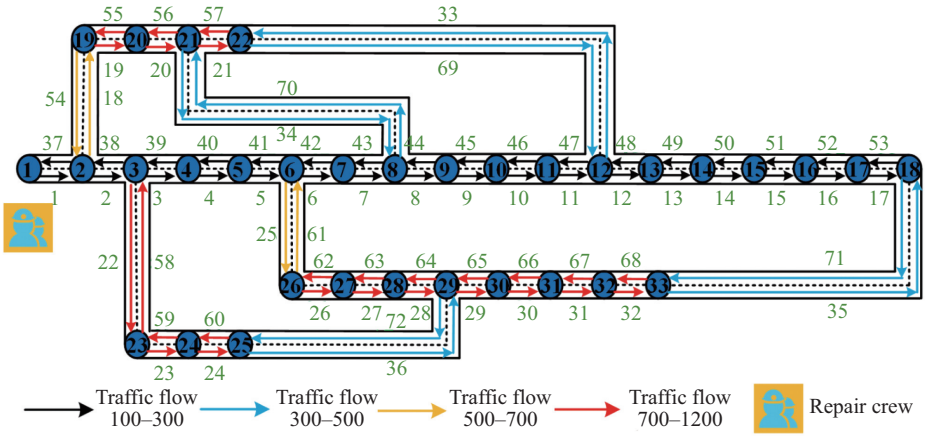

Fig. 7. The transportation system corresponding to the distribution system.

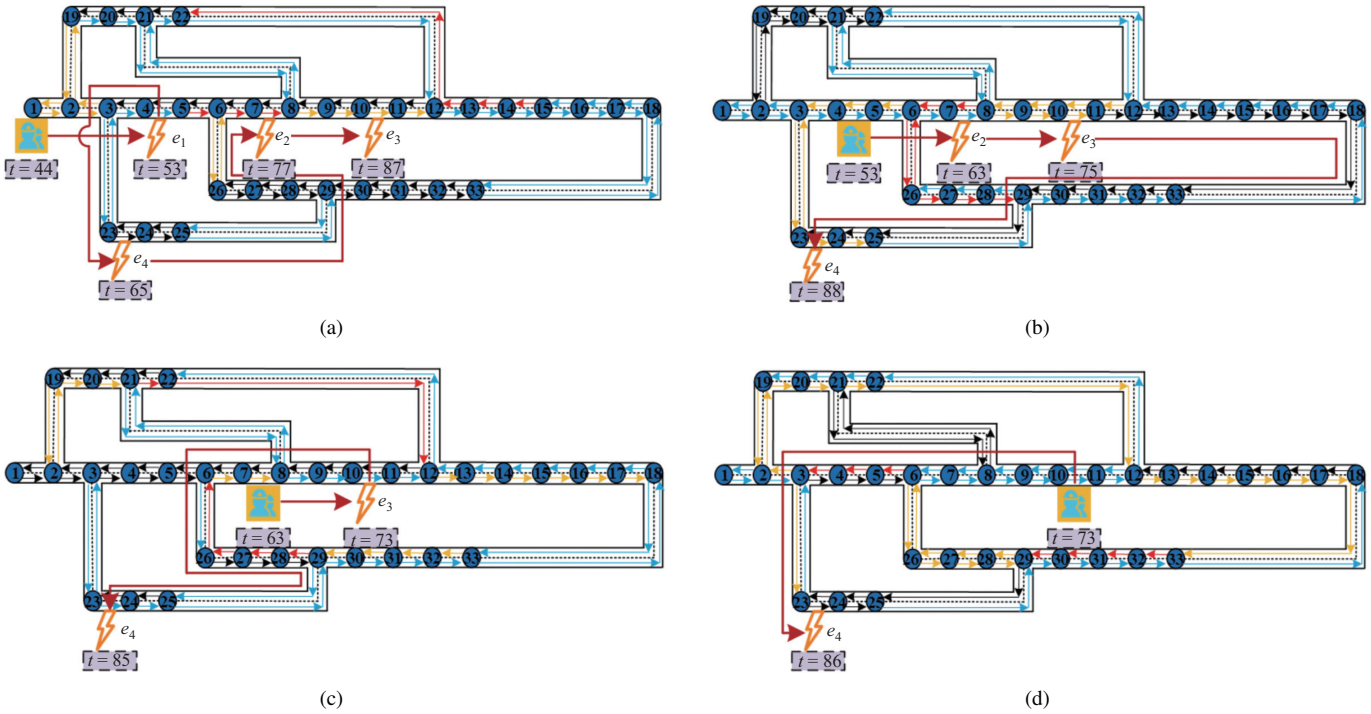

Fig. 8. Repair route of the repair crew (MTSRS). (a) $t = 44$; (b) $t = 53$; (c) $t = 63$; (d) $t = 73$.

number of faulty lines, output of distributed generators and charging/discharging of energy storages are shown in Figs. 11 and 12, respectively. The predicted target value is \$19664.4, and the calculation time is 263.29 s.

When MTSS is adopted, the recovery time matrix, optimal repair sequence, estimated repair completion time, and repair route of the repair crew are the same as the MTSRS result after multi-time-section decision-making in Stage I and Stage II, as shown in Fig. 8. Load reduction and the number of faulty lines, output of distributed generators and the charging/discharging of energy storages are shown in Figs. 13 and 14, respectively. The predicted target value is \$19124.5, and the calculation time is 327.77 s.

2) Comparative Analysis of Repair Sequence and Route

The comparison of Fig. 8(a) and Fig. 8(b)–(d) indicates that STSS will always dispatch the repair crew according to the decision plan at time t_0, and no longer update or modify the repair sequence. In contrast, MTSRS and MTSS will take the influence of uncertainties into account, as shown in Fig. 8(b). When faulty equipment $\mathrm{e}(1)$ is repaired at time $t = 53$, current traffic flow in the cells 22, 39, and 40 are increased. If the repair crew still follows the original repair sequence, travel time to the faulty equipment $\mathrm{e}(4)$ will be greatly increased. At this moment, MTSRS and MTSS will re-predict recovery time of the remaining faults $\{\mathrm{e}(i)|(7,8),(10,11),(23,24)\}$. After the optimal decision, the repair order is updated as $\mathrm{e}(2) \rightarrow \mathrm{e}(3) \rightarrow \mathrm{e}(4)$, and the repair is expected to be completed at $t = 63$, $t = 75$ and $t = 86$, respectively. After that, when the faulty equipment $\mathrm{e}(2)$ and $\mathrm{e}(3)$ are repaired at time $t = 63$ and $t = 73$, uncertain information will be updated again. Then the repair crew will re-select a better route: cell 10 $\rightarrow$ cell 9

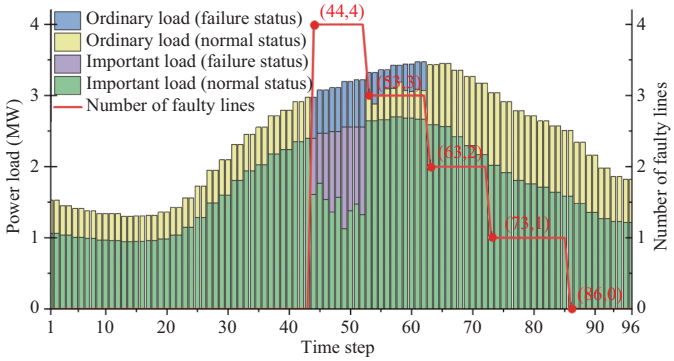

Fig. 9. Load reduction and the number of faulty lines (MTSRS).

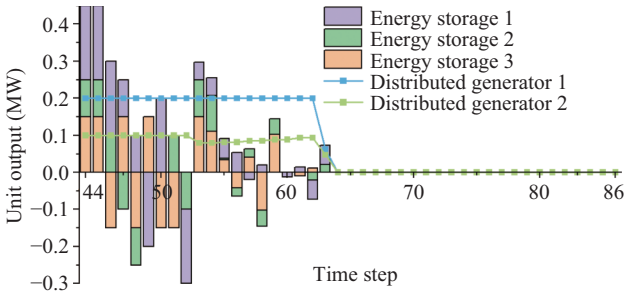

Fig. 10. Distributed generators output and energy storages state (MTSRS).

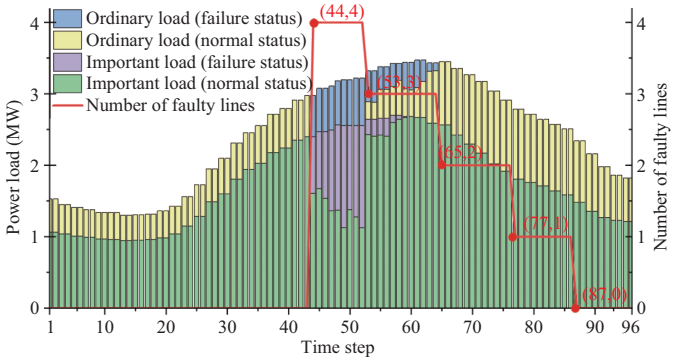

Fig. 11. Load reduction and the number of faulty lines (STSS).

$\rightarrow \cdots \rightarrow$ cell 3 $\rightarrow$ cell 23. Finally, all faulty equipment is repaired at $t = 86$, as shown in Fig. 8(d).

3) Comparative Analysis of Load Reduction and Restoration Resource Scheduling

Comparing Figs. 9, 11 and 13, we can observe that MTSRS reduces total economic losses by \$2095.4 and \$1555.4 than STSS and MTSS, respectively. Particularly, MTSRS can reduce reduction of critical industrial load (the purple part in the figure) effectively. This is because MTSRS can not only update the ultra-short-term forecast with the uncertain information many times, but also fully updates the restoration resources scheduling plan from a long-time scale. Comparing Figs. 10 and 14, it can be observed that temporal-coupling characteristics of energy storages are not considered in the scheduling plan of MTSS. The reason is that MTSS is a partial optimization of multiple time sections. In the process of repairing faulty equipment $\mathrm{e}(1)$ ($t : 40 \sim 53$), in order to

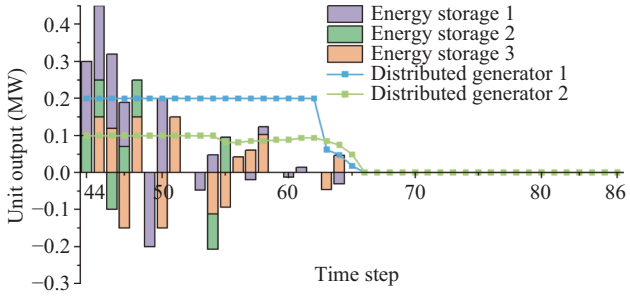

Fig. 12. Distributed generators output and energy storages state (STSS).

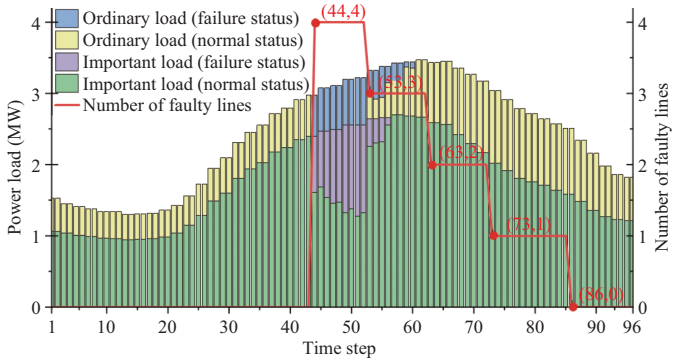

Fig. 13. Load reduction and the number of faulty lines (MTSS).

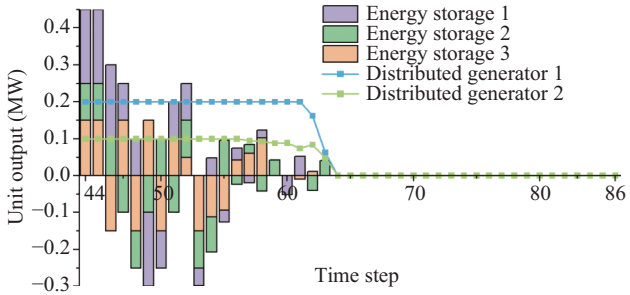

Fig. 14. Distributed generators output and energy storages state (MTSS).

minimize load reduction during this period, the SOC of the three energy storages all dropped to a relatively lower level at $t = 53$. Thus, during the first three time periods ($t : 54 \sim 56$) for repairing the faulty equipment $\mathrm{e}(2)$, energy storage can only be in a state of charging or idling. As a result, reduction of critical industrial load is larger than of MTSRS, which reflects the scheduling plan formulated by MTSS cannot achieve the global optimum.

In addition, the topology of the distribution network at some certain moments of the three strategies is shown in Table B1.

4) Comparative Analysis of Prediction Errors

In the actual repair process, when the repair sequence and load recovery plan formulated by STSS, MTSS or MTSRS are used, due to the error between the predicted value of the uncertainties and the actual value, the predicted target value calculated by the simulation will always have a certain deviation from the actual target value in the actual execution process. Therefore, this subsection tests the difference between the predicted value and the actual value of the three strategies

TABLE I
THE INFLUENCE OF UNCERTAINTIES PREDICTION ERROR ON THREE STRATEGIES

Strategies	STSS	MTSS	MTSRS
obj_{predict} (\$)	19664.4	21451.7	22779.0
obj_{real} (\$)	23662.1	23217.5	23132.8
χ	0.203	0.0823	0.0153

under the error value $\kappa = 8\%$. Results are as shown in Table I.

Among them, the deviation $\chi = |obj_{\text{predict}} - obj_{\text{real}}|/obj_{\text{predict}}$. Comparing the deviation calculation results of the three strategies, it can be found that at the same error value, the deviation of the MTSRS test results is smaller than of STSS and MTSS. Since MTSRS can make multiple rolling decisions on the repair plan based on updated information, the simulation process is closer to the actual execution process and the gap between the predicted target value and the actual target value is smaller.

C. Sensitivity Analysis of MTSRS

In order to test the sensitivity of MTSRS to uncertainties and time steps, this subsection set the errors to be $\kappa = 5\%$, 10%, 15% and time steps to be $\Delta t = 15$, 30, 60 min. Test results are shown in Table II.

TABLE II
SENSITIVITY ANALYSIS RESULTS OF MTSRS

Test group	obj_{predict} (\$)	obj_{real} (\$)	Solve time (s)	χ
$\kappa = 5\%$, $\Delta t = 15$ min	22110.7	22587.2	496.8	0.0211
$\kappa = 5\%$, $\Delta t = 30$ min	12550.9	12996.3	183.6	0.0355
$\kappa = 5\%$, $\Delta t = 60$ min	3049.6	3257.7	52.4	0.0682
$\kappa = 10\%$, $\Delta t = 15$ min	24842.8	26632.1	463.4	0.0720
$\kappa = 10\%$, $\Delta t = 30$ min	14453.9	15831.6	175.4	0.0953
$\kappa = 10\%$, $\Delta t = 60$ min	3611.2	3998.8	49.3	0.1073
$\kappa = 15\%$, $\Delta t = 15$ min	28281.0	31211.8	546.8	0.1036
$\kappa = 15\%$, $\Delta t = 30$ min	16520.8	18723.0	158.2	0.1333
$\kappa = 15\%$, $\Delta t = 60$ min	4172.5	4782.1	50.4	0.1461

Note: Because the number of value points in the target value calculation process is different under different solution time steps, namely, there is no comparative value among different solution time steps, and there is no multiple relationship.

The following conclusions can be drawn from the above table:

1) Under the same error level κ, the deviation χ becomes lower with the decrease of solution time step Δt. However, the solution time also increases significantly. This is because with shortening of the time step, the system can fully schedule various restoration resources, so the predicted target value obj_{predict} better matches the actual target value obj_{real}.

2) Under the same time step Δt, the deviation χ becomes larger with increase of the prediction error of the uncertainties. The reason is within a certain error level, MTSRS can better reduce the gap between predicted value and actual value. However, when the error is large, data updated during each rolling decision is no longer useful, and the multi-time-step rolling optimization strategy will also lose its accuracy.

VII. CONCLUSION

This paper proposes a practical scheduling plan for faulty equipment and restoration resources and a novel solution for further improving resilience of the distribution system. Based on the case study result, two conclusions can be drawn as follows:

(1) Considering variation of traffic flow affects the driving route of the repair crew, adopting a multi-time-step rolling optimization strategy can update uncertain information multiple times, which can achieve the goal of planning a shorter path for the repair crew and shortening the total duration of fault recovery.

(2) When the prediction error of traffic flow is large, the error will cause the rolling optimization strategy to lose its advantage of solution accuracy. The rise of traffic flow will increase travel time of the repair crew, which will greatly enlarge the economic loss of the system.

In future work, it is significant to study how to optimize the allocation of a repair crew and various emergency resources before disasters under the impact of the transportation network.

REFERENCES

[1] W. S. Wang, W. F. Lin, G. Q. He, W. H. Shi, and S. L. Feng, "Enlightenment of 2021 Texas blackout to the renewable energy development in China", *Proceedings of the CSEE*, vol. 41, no. 12, pp. 4033–4042, Jun. 2021.

[2] A. Gholami, F. Aminifar, and M. Shahidehpour, "Front lines against the darkness: Enhancing the resilience of the electricity grid through microgrid facilities," *IEEE Electrification Magazine*, vol. 4, no. 1, pp. 18–24, Mar. 2016.

[3] Y. Xu, J. H. He, Y. Wang, J. X. Li, and C. C. Li, "A review on distribution system restoration for resilience enhancement," *Transactions of China Electrotechnical Society*, vol. 34, no. 16, pp. 3416–3429, Aug. 2019.

[4] X. C. Huang, Y. Yang, and W. B. Fan, "Combined optimization model for maintenance scheduling and service restoration of distribution system," *Automation of Electric Power Systems*, vol. 38, no. 11, pp. 68–73, Jun. 2014.

[5] Y. Wang, Y. Xu, J. H. He, C. C. Liu, K. P. Schneider, M. G. Hong, and D. T. Ton, "Coordinating multiple sources for service restoration to enhance resilience of distribution systems," *IEEE Transactions on Smart Grid*, vol. 10, no. 5, pp. 5781–5793, Sep. 2019.

[6] B. Chen, C. Chen, J. H. Wang, and K. L. Butler-Purry, "Sequential service restoration for unbalanced distribution systems and microgrids," *IEEE Transactions on Power Systems*, vol. 33, no. 2, pp. 1507–1520, Mar. 2018.

[7] L. Che and M. Shahidehpour, "Adaptive formation of microgrids with mobile emergency resources for critical service restoration in extreme conditions," *IEEE Transactions on Power Systems*, vol. 34, no. 1, pp. 742–753, Jan. 2019.

[8] B. Chen, Z. G. Ye, C. Chen, J. H. Wang, T. Ding, and Z. H. Bie, "Toward a synthetic model for distribution system restoration and crew dispatch," *IEEE Transactions on Power Systems*, vol. 34, no. 3, pp. 2228–2239, May 2019.

[9] A. Arif, Z. Y. Wang, J. H. Wang, and C. Chen, "Power distribution system outage management with co-optimization of repairs, reconfiguration, and DG dispatch," *IEEE Transactions on Smart Grid*, vol. 9, no. 5, pp. 4109–4118, Sep. 2018.

[10] S. Y. Ge, C. H. Zhang, H. Liu, and Z. Y. Xu, "Resilience enhancement strategy for distribution network considering supporting role of micro energy grid," *Power System Technology*, vol. 43, no. 7, pp. 2306–2313, Jul. 2019.

[11] S. B. Lei, J. H. Wang, C. Chen, and Y. H. Hou, "Mobile emergency generator pre-positioning and real-time allocation for resilient response to natural disasters," *IEEE Transactions on Smart Grid*, vol. 9, no. 3, pp. 2030–2041, May 2018.

[12] Z. G. Ye, C. Chen, B. Chen, and K. Wu, "Resilient service restoration for unbalanced distribution systems with distributed energy resources by leveraging mobile generators," *IEEE Transactions on Industrial Informatics*, vol. 17, no. 2, pp. 1386–1396, Feb. 2021.

[13] Y. Wang, Y. Xu, J. X. Li, C. Li, J. H. He, J. Y. Liu, and Q. Q. Zhang, "Dynamic load restoration considering the interdependencies between

power distribution systems and urban transportation systems," *CSEE Journal of Power and Energy Systems*, vol. 6, no. 4, pp. 772–781, Aug. 2020.
[14] W. X. Liu, Y. H. Wang, Q. X. Shi, Q. Yao, and H. Y. Wan, "A multi-stage restoration strategy to enhance distribution system resilience with improved conditional generative adversarial nets," *CSEE Journal of Power and Energy Systems*, doi: 10.17775/CSEEJPES.2021.09080.
[15] S. H. Yao, P. Wang, and T. Y. Zhao, "Transportable energy storage for more resilient distribution systems with multiple microgrids," *IEEE Transactions on Smart Grid*, vol. 10, no. 3, pp. 3331–3341, May. 2019.
[16] H. H. Abdeltawab and Y. A. R. I. Mohamed, "Mobile energy storage scheduling and operation in active distribution systems," *IEEE Transactions on Industrial Electronics*, vol. 64, no. 9, pp. 6828–6840, Sep. 2017.
[17] S. B. Lei, C. Chen, H. Zhou, and Y. H. Hou, "Routing and scheduling of mobile power sources for distribution system resilience enhancement," *IEEE Transactions on Smart Grid*, vol. 10, no. 5, pp. 5650–5662, Sep. 2019.
[18] X. J. Lü, L. J. Yang, and L. D. Chen, "The summary of research on fault repair-recovery strategy for distribution network," *Journal of Hebei Normal University of Science Technology*, vol. 33, no. 1, pp. 63–66, Mar. 2019.
[19] Y. Y. Xie, Z. T. Yang, S. Cai, D. Wang, X. Chen, and Y. Zou, "Power supply restoration strategy for distribution network based on robust model prediction control," *Automation of Electric Power Systems*, vol. 45, no. 23, pp. 123–131, Dec. 2021.
[20] Y. C. Zhang and S. W. Xie, "Coordinated optimization framework of multi-timescale restoration strategies for resilience enhancement of distribution networks," *Automation of Electric Power Systems*, vol. 45, no. 18, pp. 28–34, Sep. 2021.
[21] A. Arif, S. S. Ma, Z. Y. Wang, J. H. Wang, S. M. Ryan, and C. Chen, "Optimizing service restoration in distribution systems with uncertain repair time and demand," *IEEE Transactions on Power Systems*, vol. 33, no. 6, pp. 6828–6838, Nov. 2018.
[22] A. Arif, Z. Y. Wang, C. Chen, and J. H. Wang, "Repair and resource scheduling in unbalanced distribution systems using neighborhood search," *IEEE Transactions on Smart Grid*, vol. 11, no. 1, pp. 673–685, Jan. 2020.
[23] E. F. Camacho and C. Bordons, "*Model predictive control*," in *Advanced Textbooks in Control and Signal Processing*. London, U.K.: Springer, 2004, pp. 1–4.
[24] H. B. Bao, H. Wei, X. X. Guo, and B. Li, "Model and algorithm of probabilistic interval power flow considering wind power uncertainty," *Proceedings of the CSEE*, vol. 37, no. 19, pp. 5633–5642, Oct. 2017.
[25] C. F. Daganzo, "The cell transmission model, part II: network traffic," *Transportation Research Part B: Methodological*, vol. 29, no. 2, pp. 79–93, Apr. 1995.
[26] Y. Xu, Y. Wang, J. H. He, M. Y. Su, and P. H. Ni, "Resilience-oriented distribution system restoration considering mobile emergency resource dispatch in transportation system," *IEEE Access*, vol. 7, pp. 73899–73912, 2019.
[27] Y. Zheng, Y. C. Du, and L. J. Sun, "Considerations on problems in the BPR function," *Traffic and Transportation*, vol. 23, no. S1, pp. 24–26, 2007.
[28] M. Baran and F. F. Wu, "Optimal sizing of capacitors placed on a radial distribution system," *IEEE Transactions on Power Delivery*, vol. 4, no. 1, pp. 735–743, Jan. 1989.
[29] M. E. Baran and F. F. Wu, "Optimal capacitor placement on radial distribution systems," *IEEE Transactions on Power Delivery*, vol. 4, no. 1, pp. 725–734, Jan. 1989.
[30] L. W. Gan, N. Li, U. Topcu, and S. H. Low, "Exact convex relaxation of optimal power flow in radial networks," *IEEE Transactions on Automatic Control*, vol. 60, no. 1, pp. 72–87, Jan. 2015.
[31] H. G. Yeh, D. F. Gayme, and S. H. Low, "Adaptive VAR control for distribution circuits with photovoltaic generators," *IEEE Transactions on Power Systems*, vol. 27, no. 3, pp. 1656–1663, Aug. 2012.
[32] Q. X. Shi, F. X. Li, M. Olama, J. Dong, Y. S. Xue, M. Starke, C. Winstead, and T. Kuruganti, "Network reconfiguration and distributed energy resource scheduling for improved distribution system resilience," *International Journal of Electrical Power & Energy Systems*, vol. 124, pp. 106355, Jan. 2021.
[33] T. Ding, Y. L. Lin, Z. H. Bie, and C. Chen, "A resilient microgrid formation strategy for load restoration considering master-slave distributed generators and topology reconfiguration," *Applied Energy*, vol. 199, pp. 205–216, Aug. 2017.

Haiyang Wan received a B.S. degree in North China Electric Power University, Beijing, China in 2021. He is now pursuing a Ph.D. degree in North China Electric Power University. His research interests include resilience analysis in urban power system.

Wenxia Liu received a B.S. degree in Radio Technology from Nanjing University of Science and Technology in 1990, and obtained an M.S. degree and Ph.D. degree in Electrical Engineering and Automation from Northeast of China Electrical power University and North China Electrical Power University in 1995 and 2009, respectively. She is currently Professor in the School of Electrical and Electronic Engineering, North China Electrical Power University, Beijing, China. Her research interests include risk assessment in power systems, power system dispatch and management automation.

Qingxin Shi received B.S. and M.Sc. degrees in Zhejiang University, China, and University of Alberta, Canada, in 2011 and 2014, respectively. He received a Ph.D. degree in University of Tennessee, Knoxville, USA, in 2019, where he worked as a Research Assistant Professor from 2019 to 2020. Currently, he is an Assistant Professor in the School of Electrical and Electronic Engineering, North China Electric Power University, Beijing, China. His research interests include demand response and distribution system resilience.

Yiwei Zhang received his B.S. degree in Electrical Engineering from North China Electric Power University in 2017. Currently, he is studying in State Laboratory for Alternate Electrical Power System with Renewable Energy Sources, North China Electric Power University, where he is currently pursuing a Ph.D. degree in Electrical Engineering. His research interests include vulnerability and resilience of cyber-physical systems.

Yuehan Wang received a B.S. degree in North China Electric Power University, Beijing, China in 2020. He is now pursuing an M.S. degree in North China Electric Power University. His research interests include distribution system resilience and operation.

Shuai Zhang received a B.S. degree in XingTai University, China in 2016 and obtained an M.S. degree in Beijing Information Science and Technology University, Beijing, China in 2019. He is now pursuing a Ph.D. degree in North China Electric Power University. His research interests include power system reliability evaluation.